Magnet-Induced Temporary Superhydrophobic Coatings from One-Pot Synthesized Hydrophobic Magnetic Nanoparticles

Jian Fang, Hongxia Wang, Yuhua Xue, Xungai Wang, and Tong Lin*

Centre for Material and Fibre Innovation, Deakin University, Geelong, Victoria 3217, Australia

ABSTRACT In this paper, we report on the production of superhydrophobic coatings on various substrates (e.g., glass slide, silicon wafer, aluminum foil, plastic film, nanofiber mat, textile fabrics) using hydrophobic magnetic nanoparticles and a magnet-assembly technique. Fe_3O_4 magnetic nanoparticles functionalized with a thin layer of fluoroalkyl silica on the surface were synthesized by one-step coprecipitation of Fe^{2+}/Fe^{3+} under an alkaline condition in the presence of a fluorinated alkyl silane. Under a magnetic field, the magnetic nanoparticles can be easily deposited on any solid substrate to form a thin superhydrophobic coating with water contact angle as high as 172°, and the surface superhydrophobicity showed very little dependence on the substrate type. The particulate coating showed reasonable durability because of strong aggregation effect of nanoparticles, but the coating layer can be removed (e.g., by ultrasonication) to restore the original surface feature of the substrates. By comparison, the thin particle layer deposited under no magnetic field showed much lower hydrophobicity. The main reason for magnet-induced superhydrophobic surfaces is the formation of nano- and microstructured surface features. Such a magnet-induced temporary superhydrophobic coating may have wide applications in electronic, biomedical, and defense-related areas.

KEYWORDS: superhydrophobic • magnetic nanoparticles • one-pot synthesis • temporary coating • magnet-induced superhydrophobicity

INTRODUCTION

Recently, considerable research has been focused on superhydrophobicity and its novel applications. Besides the well-known nonsticking function for self-cleaning application, superhydrophobic surfaces have been shown many new applications in areas such as oil-water separation (1), energy conversion (2−4), protection of electronic devices in a high moisture environment (5), controlling cell adhesion on substrate surface (6, 7), reducing fluid resistance for aquaculture devices (8), and reduction of fluid drag in microfluidic devices (9, 10).

For many of the applications, superhydrophobicity is required only temporarily. It is expected that a temporary superhydrophobic surface can be generated and removed easily on demand. Take a microfluidic device as an example. Hydrophobicity has been used as passive valves for controlling the fluid motion in microfluidic devices (11). If a temporary valve can be applied and removed easily, one microfluidic device can be set to have different flow routes, depending on the location and profile of the valves set in the microfluidic channels, which makes the microfluidic device universal for different purposes. Temporary superhydrophobicity is also useful for smart batteries (12), liquid droplet manipulation (e.g. liquid marbles) (2), bioelectrocatalysis (13), and cell culturing (7).

One approach to realize on-demand surface superhydrophobicity is through switchable superhydrophobic coatings that can change between superhydrophobicity and hydrophilicity reversibly under an external stimulus such as UV light, thermal, and electrical fields (14−19). Most of the switchable superhydrophobic coatings, however, are either difficult to prepare or only suitable for specific substrates (e.g. silicon wafer), which restrict their wide applications. Superhydrophobic materials that can be coated on any solid substrate to form superhydrophobic surface and removed easily so that the original substrate surface can be restored are highly desired, but hasn't been demonstrated in the research literature.

Magnetic nanoparticles (MNPs) are ideal to make remotely controllable or switchable devices because of the intrinsic prompt response to an external magnetic field. They have been used broadly in medical imaging (20), controlled target drug or gene delivery (21, 22), hyperthermia treatment of cancerous tumors (23), chemical and bioseparations (24, 25), information storage (26, 27), and catalysis (28). To enhance the dispersion stability, biocompatibility, target specificity, and chemotherapeutic function, most of magnetic nanoparticles are surface modified. To this end, core−shell structured MNPs are normally employed (29, 30), which require a complicated fabrication process. One-pot synthesis of functional MNPs is highly preferred because of the simplified experiment procedure and ability to avoid particle agglomeration arising from incomplete surface treatment (31). Recently, magnetic nanoparticles

* Corresponding author.
Received for review February 3, 2010 and accepted April 6, 2010
DOI: 10.1021/am100092b

Scheme 1. Synthesetic Route for Surface-Functionalized Fe_3O_4 Nanoparticles

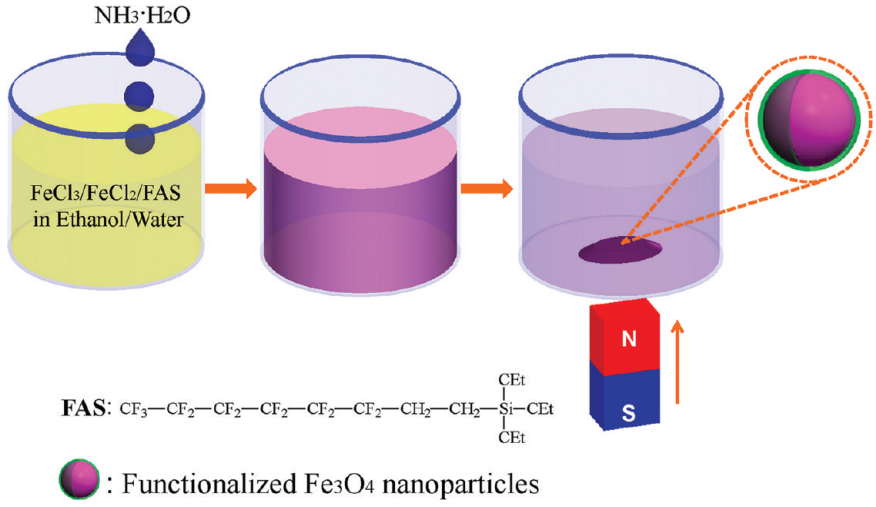

have been used to improve the adhesion of microdroplets on a non-wetting superhydrophobic iron surface (32). The droplets containing superparamagnetic nanoparticles stuck on the superhydrophobic iron surface when the nanoparticles were magnetized by an external magnetic field. When the superparamagnetic nanoparticles were demagnetized, the droplet got repelled and thus detached from the surface. This novel surface has potential applications in biochemical separation, no-loss microdroplet transport and in situ detection.

In this paper, we have for the first time demonstrated that temporary superhydrophobic surfaces can be generated universally by magnetic deposition of one-pot synthesized hydrophobic magnetic nanoparticles on various solid surfaces. We have found that the magnet assisted assembly process is essential for the formation of a thin superhydrophobic coating (thickness less than 50 μm) because of the novel surface morphology, and that the superhydrophobic coating shows reasonable durability during use but can be eliminated by an ultrasonication process.

EXPERIMENTAL SECTION

Materials. Ethanol and ferric(III) chloride hexahydrate ($FeCl_3 \cdot 6H_2O$) were purchased from Aldrich. Ammonia solution (25% NH_3 in water) and ferrous(II) chloride tetrahydrate ($FeCl_2 \cdot 4H_2O$) were obtained from Merck. Tridecafluorooctyl triethoxysilane (FAS, Dynasylan F 8261) was supplied by Degussa.

Synthesis of Pure and Hydrophobic MNPs. Pure Fe_3O_4 nanoparticles were prepared by coprecipitating Fe^{2+} and Fe^{3+} ions in aqueous ammonia solution. To 200 mL of deionized water containing 0.85 g of ferric chloride and 0.30 g of ferrous chloride (molar ratio 2:1) was dropped 1.5 M NH_4OH solution under a N_2 atmosphere while the solution was stirred rapidly. The solution was controlled at pH 8 by adjusting the speed of adding NH_4OH. The resulting precipitate was stirred for 2 h. After triple washes with deionized water and ethanol the precipitates were re-suspended in 100 mL deionized water. The pure magnetic nanoparticles were isolated from the solution by a magnet bar. The surface functionalized hydrophobic nanoparticles were synthesized using a similar procedure except that the NH_4OH solution was dropped into 200 mL of ethanol-water solution (1/4 in volume) containing 0.85 g of ferric chloride, 0.30 g of ferrous chloride (molar ratio 2:1), and 0.2 mL of FAS.

Formation of Superhydrophobic Surfaces. Superhydrophobic surfaces were prepared by a magnet-induced particle deposition method: a permanent magnet (neodymium cylinder magnets, Ø8×15 mm (AMF magnetics)) was used to induce the deposition of MNPs onto the desired area of the substrates. Once the MNPs were deposited onto the substrate surface, the solvent was removed and the MNP coating was dried under ambient condition. To examine the universality of this treatment, several substrates have been used, including glass slide, silicon wafer, polished aluminum foil, PET film, polyacrylonitrile (PAN) nanofiber mat (fiber diameter: 197 ± 21 nm), cotton fabric (plain weave, 160 g/m^2), and polyester fabric (plain weave, 168 g/m^2). For comparison, the nanoparticles were also deposited using the same procedure except that no magnetic field was applied. In the paper, such a coating method is called "normal deposition process" or "normal coating method".

Characterizations. Scanning electron microscopy (SEM, ZEISS Supra 55VP) and transmission electron microscopy (TEM, FEI Tecnai F30 Cryo TEM) was used to observe the magnetic nanoparticles. Water contact angles were measured using a contact angle meter (CAM101 KSV). Atomic force microscopy (AFM) imaging was performed on a Nanoscope III multimode scanning probe microscope (Digital Instruments, Santa Barbara) operating in the tapping mode in air. Root-mean-square (rms) roughness was analyzed from AFM height images using the Nanoscope software version 5.30b4. Fourier transform infrared spectra (FTIR) were measured on a FTIR spectrometry (Bruker Optics) in ATR mode. X-ray diffraction (XRD) was performed on a powder diffractometer (Philips 1140/90) using Cu radiation 1.54 Å. The samples were analyzed at room temperature over a 2θ range of 10−80° with sampling intervals of 0.02° and a scanning rate of 1°/min. X-ray photoelectron spectroscopy(XPS) data was acquired using a Kratos AXIS Ultra DLD X-ray photoelectron spectrometer incorporating a 165 mm hemispherical electron energy analyzer. The incident radiation was Monochromatic Al X-rays (1486.6 eV) at 150W (15 kV, 10 mA). The obtained spectra were analyzed by the CasaXPS software. Magnetic properties ($M-H$ curves) were measured at room temperature (300 K) with a Quantum Design MPMS-5 DC-SQUID (superconducting quantum interference device) susceptometer.

RESULTS AND DISCUSSION

The procedure for one-pot synthesis of hydrophobic Fe_3O_4 nanoparticles is depicted in Scheme 1. Fe^{2+}/Fe^{3+} salts in an ethanol−water solution containing FAS were coprecipitated by adding $NH_3 \cdot H_2O$ to the solution. Brown particles formed immediately once the $NH_3 \cdot H_2O$ solution was dropped into the reactant solution, and the resultant solid

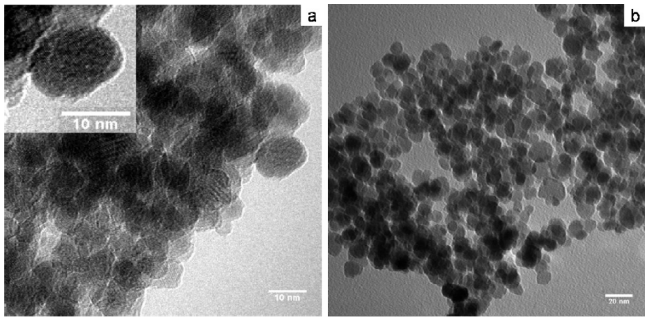

FIGURE 1. TEM images of as-synthesized (a) surface functionalized and (b) pure Fe_3O_4 nanoparticles.

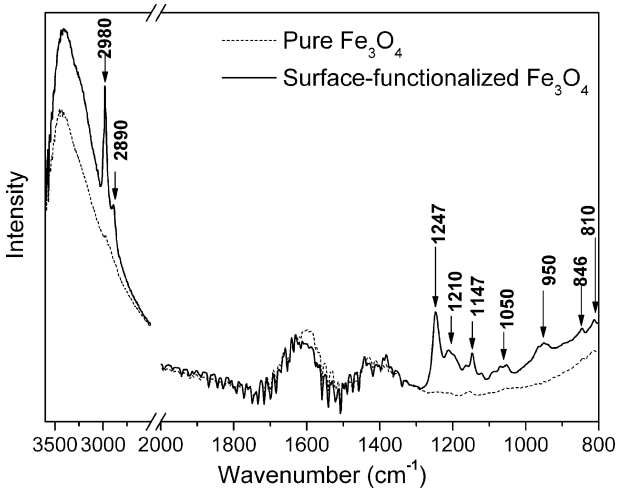

FIGURE 2. FTIR spectra of pure and surface-functionalized Fe_3O_4 nanoparticles.

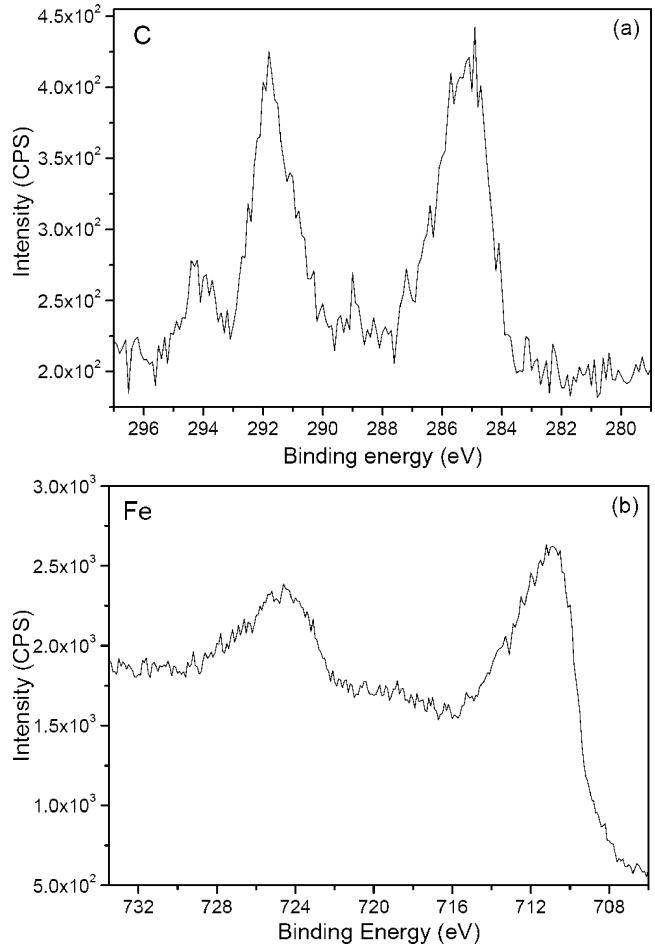

FIGURE 3. High-resolution XPS spectra of (a) C1s and (b) Fe2p of the surface-functionalized Fe_3O_4 nanoparticles.

product showed magnetic response, because they can be attracted by a permanent magnet bar easily.

Figure 1 shows the TEM images of typical Fe_3O_4 nanoparticles synthesized in this study. These particles looked uniform with an average nanoparticle size of about 9.97 nm and a narrow size distribution (standard deviation, 0.89 nm). The inset image in Figure 1a reveals that some particles have a core-shell structure with the shell thickness up to 2 nm. However, the shell layer for many other nanoparticles was too thin to be observed. Further work is warrant to find an effective way to control the shell thickness through synthesis. For comparison, the morphology of pure Fe_3O_4 nanoparticles synthesized under the same condition but without FAS in the reaction solution is shown in Figure 1b. The average size of the pure Fe_3O_4 nanoparticles, based on TEM images, was 9.92 nm, which is very close to that of the surface-functionalized nanoparticles.

The FTIR spectra of the as-prepared nanoparticles are shown in Figure 2. The surface-functionalized nanoparticles showed new FTIR vibration peaks when compared with the pure nanoparticles. The peaks at 1050 and 810 cm^{-1} correspond to the Si−O−Si asymmetrical stretching and bending vibrations (33, 34). The peak at 846 cm^{-1} was the C−Si stretching vibration. Three peaks at 1147, 1210, and 1247 cm^{-1} were due to C−F stretching vibrations (35), and the parks at 2890 and 2980 cm^{-1} correspond to C−H stretching of the $-CH_2$ units (36−38), the characteristics of which are in good accordance with the FTIR spectrum of pure FAS (see the Supporting Information, Figure S1). These results indicated the formation of fluorinated silica on the surface-functionalized particles.

The XPS measurement further confirmed the chemical composition of the surface functionalized nanoparticles. New peaks of F, C and Si elements appeared in the XPS survey spectrum (see the Supporting Information, Figure S2) of the hydrophobic nanoparticles. The molar ratio of elements F and Fe based on the survey spectrum was 19.60: 17.97 F:Fe (mol/mol). It should be noted that the working distance of XPS analysis is about 10 nm from the specimen surface, and the size of our particles in the specimen is also within this range; therefore, the ratio reflects the overall chemical composition of the particles, and not just the particle surface. The C1s in high-resolution spectra showed the binding energies at 294, 292, 289, and 285 eV (Figure 3a), which are typical for $-CF_3$ $-CF_2$, −CF, and −CH moieties, respectively (39−42). The binding energies at 724 and 710 eV are characteristic of $Fe2p_{1/2}$ and $Fe2p_{3/2}$ of Fe_3O_4 (Figure 3b).

Figure 4 shows the XRD patterns of the pure and the surface-functionalized Fe_3O_4 nanoparticles. Both curves look similar and they have diffraction peaks at $2\theta = 18.6$, 30.4, 35.7, 43.2, 53.7, 57.3, 62.8, 71.4, and 74.5°, which can be indexed respectively to the (111), (220), (311), (400), (422),

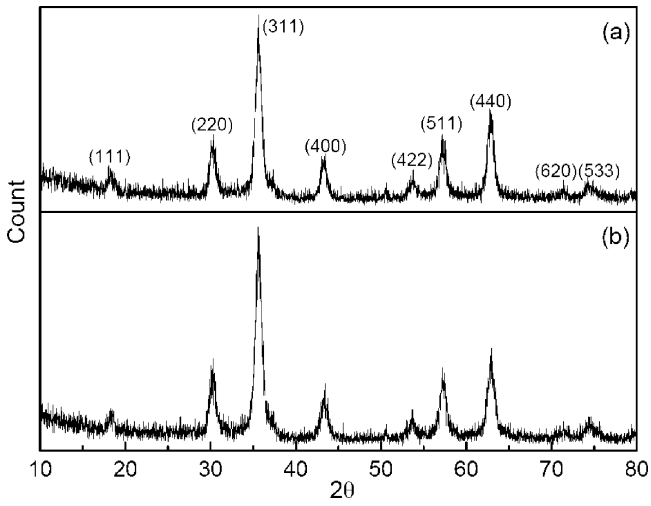

FIGURE 4. XRD patterns of (a) pure and (b) surface-functionalized Fe_3O_4 nanoparticles.

(511), (440), (620), and (533) planes of Fe_3O_4 in a face-centered cubic Fe_3O_4. The similar XRD pattern suggested that crystalline characteristic of the resultant surface-functionalized Fe_3O_4 nanoparticles was similar to that of the pure MNPs, and therefore the presence of FAS in the reaction had little influence on the crystalline characteristic of the Fe_3O_4 particles, and the silica layer should be formed on the Fe_3O_4 particle surface. The particle size calculated by the Scherrer's formula (43) based on the reflection peak of (311) was 8.4 ± 0.8 nm and 8.6 ± 0.7 nm for the pure and surface-functionalized Fe_3O_4 nanoparticles, respectively, which is very close to the values obtained from the TEM images.

The magnetic properties of the surface functionalized Fe_3O_4 nanoparticles were examined and compared with those of the pure Fe_3O_4 nanoparticles. As shown in Figure 5a, there is no visible difference in the shape of the zero-field-cooled (ZFC) and field-cooled (FC) curves and both kinds of particles have similar blocking temperatures. Both samples also showed standard paramagnetic characteristic curves (Figure 5b) with no hysteresis appearing after removal of the applied magnetic field. The saturation magnetization of pure Fe_3O_4 nanoparticles was found to be 65.20 emu/g at 300K, which is lower than the value of bulk magnetite (44). The surface functionalized Fe_3O_4 nanoparticles have a similar magnetization value with a little reduction of the saturation magnetization value, 53.10 emu/g. Even though the surface functionalized nanoparticles have a lower magnetization value, they can still be manipulated by an external magnetic field. The reduction in the magnetization value can be attributed to the thin silica layer on the nanoparticle surface. The considerable influence of functionalized surface on the magnetization value of Fe_3O_4 nanoparticles has been reported by other researchers. It has been reported that the magnetization value of Fe_3O_4 nanoparticles was reduced even the surface was covered with a single molecule layer of lipase (45), and a thick shell layer can considerably reduce the magnetization (46).

Our previous work on the synthesis of core-shell silica nanoparticles has indicated that FAS can be hydrolyzed slowly in alkaline condition to form a silica shell on faster hydrolyzed TEOS (Tetraethylortho silicate) (40). Replacing the TEOS with Fe^{2+}/Fe^{3+} salt in the existing work should lead to a similar coating on the Fe_3O_4 cores, except that the shell could be thinner because weaker alkaline condition was used.

To realize temporary superhydrophobic surface, magnet-induced particle deposition was applied on different substrates. Figure 6a shows the photo of magnet-induced coating of superhydrophobic magnetic particles on a glass slide. Using a magnet rod, the brown magnetic nanoparticles can be easily deposited to form a coating on the desired area with a similar size to the magnet. As illustrated in Figure 6b, the coated area showed very high superhydrophobicity. When a small water drop (7 μL) was placed on the coated surface, a near-spherical water droplet stood on the glass slide for a long period of time after the surface was coated with the surface-functionalized iron oxide nanoparticles. However, water can spread on the surface around the coated area on the glass slide. The contact angle (CA) measurements indicated that the coated surface had a water contact angle of 172.8 ± 0.2°. For comparison, the glass slide coated with the pure Fe_3O_4 nanoparticles using the same coating method, had a contact angle as low as 40.3 ± 0.6°. The water contact angle of the MNP coating on glass slide and other substrates are listed in Table 1. The contact angle for the surface-functionalized MNP-treated surface was in the range of 165−172°.

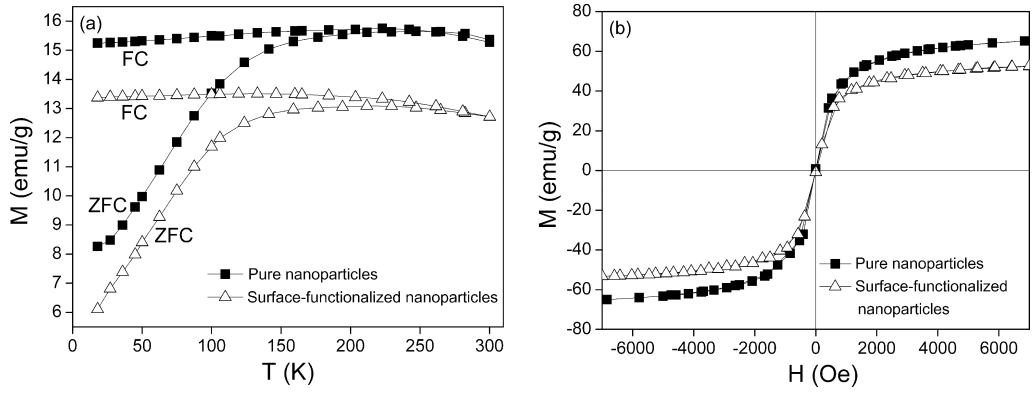

FIGURE 5. Magnetic properties of pure and surface-functionalized Fe_3O_4 nanoparticles: (a) ZFC-FC curves measured with the field of 100 Oe and (b) magnetization curve measured at 300 K.

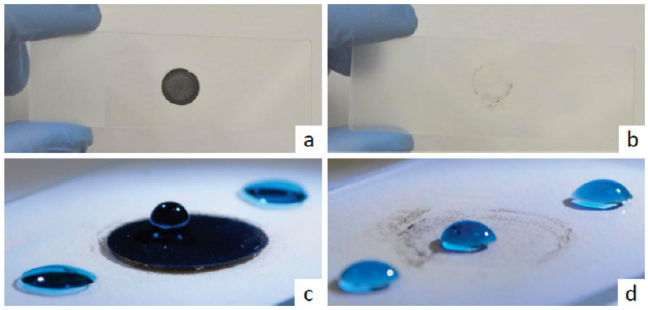

FIGURE 6. Photos of the magnet-induced coated MNPs on a glass slide (a) before and (b) after ultrasonication cleaning in ethanol, and blue water droplets on the glass slide, (c) one droplet on the coated area with two others on the uncoated area, (d) three droplets on the same spots after ultrasonication cleaning.

The magnet-induced MNP coating was very stable when a magnet rod was placed on the back, and can stand gentle rinsing and impacts. However, the coating can also be removed by ultrasonication of the coated substrates in ethanol. Figure 6c shows a water drop on a coated glass slide after 1 min ultrasonication in ethanol. As can be seen from the photo, almost all nanoparticles were cleaned from the glass slide and only a very small amount of particles left on the edge of the coated area, which can be completely removed by a longer ultrasonication treatment. After the removal of the coated particles, the glass slide showed uniform wettability and the recovered area had the same contact angle as the uncoated surface around (Figure 6d).

It was also interesting to note that if the surface-functionalized magnetite nanoparticles were applied onto the substrates using a similar deposition procedure except that no external magnetic field is used (normal coating method), almost all substrates had much lower contact angles than

Table 1. Water Contact Angles of the Substrates before and after MNP Coating Treatments

	WCA (deg)				
		surface-functionalized MNPs		pure MNPs	
substrates	uncoated	magnet-induced coating	normal coating	magnet-induced coating	normal coating
glass slide	41.2 ± 0.2	172.8 ± 0.2	124.6 ± 2.1	40.3 ± 0.6	38.9 ± 1.2
silicon wafer	61.1 ± 0.2	168.2 ± 0.1	136.3 ± 1.2	19.7 ± 0.6	55.2 ± 0.5
al foil	74.1 ± 0.3	165.8 ± 0.7	119.0 ± 0.8	25.2 ± 0.4	27.2 ± 0.6
PET film	86.7 ± 0.3	164.5 ± 0.4	113.2 ± 0.5	21.3 ± 0.3	37.1 ± 0.8
PAN nanofiber mat	109.1 ± 0.1	166.1 ± 0.4	131.5 ± 2.2	0	0
filter paper	0	170.8 ± 0.6	35.1 ± 1.1	0	0
cotton fabric	37.9 ± 0.2	165.1 ± 0.4	144.4 ± 2.4	0	20.0 ± 1.1
polyester fabric	117.1 ± 0.2	168.3 ± 0.6	165.1 ± 2.2	0	61.6 ± 0.9

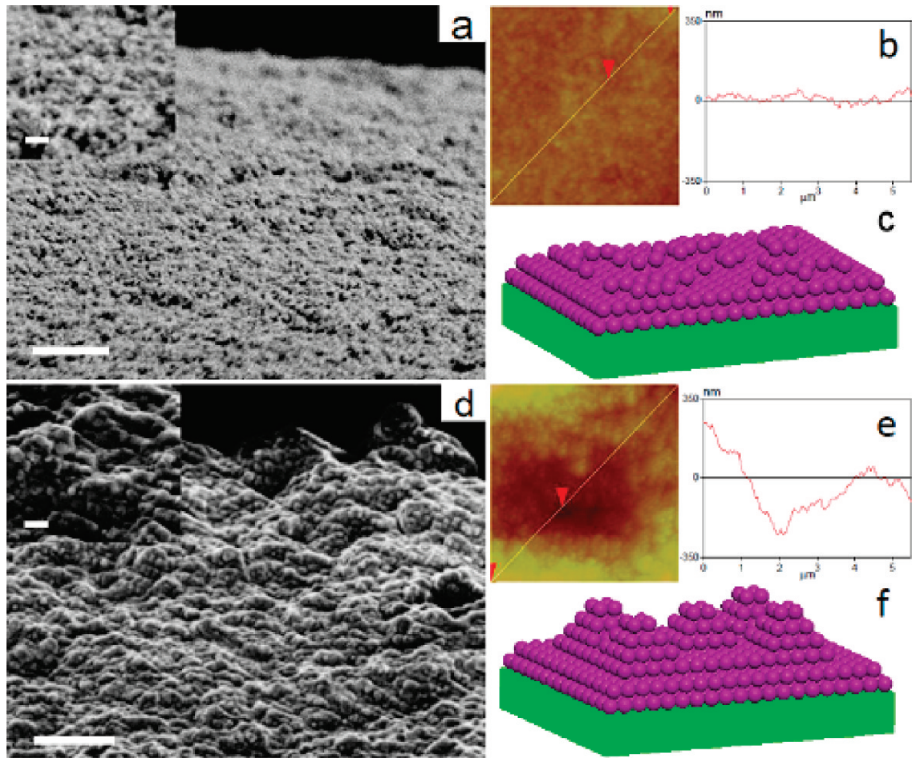

FIGURE 7. SEM and AFM (4 × 4 μm^2) images and illustrations of the coated surface. (a−c) Fe_3O_4 nanoparticles coated on silicon wafer using conventional particle deposition method; (d−f) the same amount of MNPs coated on silicon wafer using the magnet-induced particle deposition method (scale bars in SEM, 500 nm; inset scale bar, 100 nm).

those of the substrates coated by magnet-induced particle deposition (Table 1), even if the areal density of the particle coated surface is the same. One exception was the coating on polyester fabric, which had a contact angle higher than 150°. This was probably because of the integration of the intrinsic hydrophobicity of polyester and the rough surface structure from the weave patterns. It should be noted that the coating layer in our study is very thin, typically less than 50 μm. If the coating layer is thick enough (e.g., larger than 500 μm), the surface-functionalized nanoparticle coated surface can be always superhydrophobic, no matter which method is used.

To explore why the magnet aided deposition can lead to superhydrophobic surfaces, the deposited MNP coatings were observed by SEM and AFM. Without an external magnetic field, the deposition of MNPs resulted in a homogenous surface (Figure 7a–c). However, the magnet-induced particle deposition led to the formation of a rough coating surface (Figure 7d–f), presumably because the magnet domains in the magnetic bar lead to uneven deposition of MNPs under a hierarchical micro magnetic zone (47). As a result, larger agglomerated MNPs, with diameters in the range from 30 to 100 nm, protruded from the surface. AFM images show that the silicon wafer is covered with a smooth surface layer when the MNP coating was not aided by an external magnetic field (Figure 7b). However the magnet-induced particle coating showed a much rougher surface with a fluctuating cross-section profile (Figure 7e). The RMS roughness based on the AFM images was 20 nm and 159 nm for the normal and magnet-induced coating surfaces, respectively. The nanostructured rough surface induced by an external magnetic field could be the main reason leading to superhydrophobicity (48, 49).

For comparison, pure magnetic nanoparticles were also applied on the substrates using the same methods. As listed in Table 1, the magnet-induced coatings show a similar or lower water contact angle values compared to those prepared by the normal coating method.

The main reason for not forming a superhydrophobic surface by the normal coating process is that the thin nanoparticle layer deposited has a loose structure. This makes the coating have a low capillary pressure to prevent water from penetration, and the nanoparticles are also easy to move with the contacting water, leading to low hydrophobicity. In contrast, the magnet-induced coating method makes the magnetic nanoparticles aggregate strongly to form thin and dense film with a rough surface. The air bubbles trapped by such a structure are more stable, hence the non-wetting state.

CONCLUSION

We have demonstrated a simple and novel one-pot coprecipitation to synthesize hydrophobic surface functionalized iron oxide nanoparticles comprising a magnetic Fe_3O_4 core and a fluorinated silica surface. The presence of FAS during synthesis didn't influence the crystalline characteristic of the Fe_3O_4 core, but reduced the particle surface free energy. By applying an external magnetic field, the hydrophobic magnetic nanoparticles can be easily deposited on various substrates to form superhydrophobic surfaces with the water contact angles greater than 165°. The magnet-induced deposition allows easy control of the targeted areas to form a temporary superhydrophobic layer with hierarchically rough surfaces on the substrates, and this superhydrophobic coating can also be easily removed by an ultrasonication treatment. This temporary superhydrophobic coating may find applications in energy storage devices, switchable biocatalyst, and multifunctional surfaces for biomedical applications.

Acknowledgment. Funding support from Deakin University under Central Research Grant Scheme is acknowledged.

Supporting Information Available: FTIR spectrum of pure FAS and XPS survey spectrum of the surface-functionalized magnetic nanoparticles (PDF). This material is available free of charge via the Internet at http://pubs.acs.org.

REFERENCES AND NOTES

(1) Pan, Q.; Wang, M.; Wang, H. *Appl. Surf. Sci.* **2008**, *254*, 6002–6006.
(2) Bhushan, B.; Ling, X. *J. Colloid Interface Sci.* **2009**, *329*, 196–201.
(3) Lifton, V. A.; Simon, S.; Frahm, R. E. *Bell Labs Tech. J.* **2005**, *10*, 81–85.
(4) Nosonovsky, M.; Bhushan, B. *Philos. Trans. R. Soc. London, Ser. A* **2009**, *367*, 1511–1539.
(5) Samuel, J. D. J. S.; Ruther, P.; Frerichs, H. P.; Lehmann, M.; Paul, O.; Rühe, J. *Sens. Actuators, B* **2005**, *110*, 218–224.
(6) Galopin, E.; Piret, G.; Szunerits, S.; Lequette, Y.; Faille, C.; Boukherroub, R. *Langmuir* **2009**, *26*, 3479–3484.
(7) Wang, Y.; Sims, C. E.; Marc, P.; Bachman, M.; Li, G. P.; Allbritton, N. L. *Langmuir* **2006**, *22*, 8257–8262.
(8) Shi, F.; Niu, J.; Liu, J.; Liu, F.; Wang, Z.; Feng, X.-Q.; Zhang, X. *Adv. Mater.* **2007**, *19*, 2257–2261.
(9) Fukagata, K.; Kasagi, N.; Koumoutsakos, P. *Phys. Fluids* **2006**, *18*, 051703–4.
(10) Ou, J.; Rothstein, J. P. *Phys. Fluids* **2005**, *17*, 103606–10.
(11) Andersson, H.; van der Wijngaart, W.; Griss, P.; Niklaus, F.; Stemme, G. *Sens. Actuators, B* **2001**, *75*, 136–141.
(12) Lifton, V. A.; Taylor, J. A.; Vyas, B.; Kolodner, P.; Cirelli, R.; Basavanhally, N.; Papazian, A.; Frahm, R.; Simon, S.; Krupenkin, T. *Appl. Phys. Lett.* **2008**, *93*, 043112–3.
(13) Willner, I.; Katz, E. *Langmuir* **2006**, *22*, 1409–1419.
(14) Chunder, A.; Etcheverry, K.; Londe, G.; Cho, H. J.; Zhai, L. *Colloids Surf., A* **2009**, *333*, 187–193.
(15) Feng, X.; Zhai, J.; Jiang, L. *Angew. Chem., Int. Ed.* **2005**, *44*, 5115–5118.
(16) Sun, T.; Wang, G.; Feng, L.; Liu, B.; Ma, Y.; Jiang, L.; Zhu, D. *Angew. Chem., Int. Ed.* **2004**, *43*, 357–360.
(17) Verplanck, N.; Coffinier, Y.; Thomy, V.; Boukherroub, R. *Nanoscale Res. Lett.* **2007**, *2*, 577–596.
(18) Xu, L.; Chen, W.; Mulchandani, A.; Yan, Y. *Angew. Chem., Int. Ed.* **2005**, *44*, 6009–6012.
(19) Xu, L.; Chen, Z.; Chen, W.; Mulchandani, A.; Yan, Y. *Macromol. Rapid Commun.* **2008**, *29*, 832–838.
(20) Duguet, E.; Vasseur, S.; Mornet, S.; Devoisselle, J.-M. *Nanomedicine* **2006**, *1*, 157–168.
(21) Dobson, J. *Nanomedicine* **2006**, *1*, 31–37.
(22) McCarthy, J. R.; Kelly, K. A.; Sun, E. Y.; Weissleder, R. *Nanomedicine* **2007**, *2*, 153–167.
(23) Pankhurst, Q. A.; Connolly, J.; Jones, S. K.; Dobson, J. *J. Phys. D: Appl. Phys.* **2003**, *36*, R167–R181.
(24) Grass, R. N.; Athanassiou, E. K.; Stark, W. J. *Angew. Chem., Int. Ed.* **2007**, *46*, 4909–4912.
(25) Gu, H.; Xu, K.; Xu, C.; Xu, B. *Chem. Commun.* **2006**, 941–949.
(26) Bader, S. D. *Rev. Mod. Phys.* **2006**, *78*, 1–15.
(27) Sun, S.; Murray, C. B.; Weller, D.; Folks, L.; Moser, A. *Science* **2000**, *287*, 1989–1992.
(28) Wei, H.; Wang, E. *Anal. Chem.* **2008**, *80*, 2250–2254.

(29) Gupta, A. K.; Gupta, M. *Biomaterials* **2005**, *26*, 3995–4021.
(30) Salgueirino-Maceira, V.; Correa-Duarte, M. A. *Adv. Mater.* **2007**, *19*, 4131–4144.
(31) Sun, C.; Lee, J. S. H.; Zhang, M. *Adv. Drug Delivery Rev.* **2008**, *60*, 1252–1265.
(32) Cheng, Z.; Feng, L.; Jiang, L. *Adv. Funct. Mater.* **2008**, *18*, 3219–3225.
(33) Kim, M. T. *Thin Solid Films* **1997**, *311*, 157–163.
(34) Mergia, K.; Lafatzis, D.; Moutis, N.; Speliotis, T.; Apostolopoulos, G.; Cousin, F. *Appl. Phys. A* **2008**, *92*, 387–395.
(35) Hozumi, A.; Sekoguchi, H.; Kakinoki, N.; Takai, O. *J. Mater. Sci.* **1997**, *32*, 4253–4259.
(36) Kaneko, T.; Nemoto, D.; Horiguchi, A.; Miyakawa, N. *J. Cryst. Growth* **2005**, *275*, e1097–e1101.
(37) Yang, C.-S.; Bley, R. A.; Kauzlarich, S. M.; Lee, H. W. H.; Delgado, G. R. *J. Am. Chem. Soc.* **1999**, *121*, 5191–5195.
(38) Okoroanyanwu, U.; Shimokawa, T.; Byers, J.; Willson, C. G. *Chem. Mater.* **1998**, *10*, 3319–3327.
(39) Briggs, D.; Seah, M. P. *Practical Surface Analysis: by Auger and X-ray Photoelectron Spectrascopy*; Wiley: New York, 1983.
(40) Wang, H.; Fang, J.; Cheng, T.; Ding, J.; Qu, L.; Dai, L.; Wang, X.; Lin, T. *Chem. Commun.* **2008**, 877–879.
(41) Endo, K.; Tatsumi, T. *Appl. Phys. Lett.* **1996**, *68*, 2864–2866.
(42) Savage, C. R.; Timmons, R. B.; Lin, J. W. *Chem. Mater.* **1991**, *3*, 575–577.
(43) Klug, H. P.; Alexander, L. E. *X-Ray Diffraction Procedures for Polycrystalline and Amorphous Materials*; John Wiley & Sons: New York, 1974.
(44) Zaitsev, V. S.; Filimonov, D. S.; Presnyakov, I. A.; Gambino, R. J.; Chu, B. *J. Colloid Interface Sci.* **1999**, *212*, 49–57.
(45) Huang, S.-H.; Liao, M.-H.; Chen, D.-H. *Biotechnol. Progr.* **2003**, *19*, 1095–1100.
(46) Deng, Y. H.; Wang, C. C.; Hu, J. H.; Yang, W. L.; Fu, S. K. *Colloids Surf., A* **2005**, *262*, 87–93.
(47) Chikazumi, S. *Physics of Ferromagnetism*: Oxford University Press: Oxford, U.K., 1997.
(48) Koch, K.; Bhushan, B.; Jung, Y. C.; Barthlott, W. *Soft Matter* **2009**, *5*, 1386–1393.
(49) Leng, B.; Shao, Z.; With, G. d.; Ming, W. *Langmuir* **2009**, *25*, 2456–2460.

AM100092B